JOPSS
JAEA Originated Papers Searching System

日本原子力研究開発機構機関リポジトリ
Japan Atomic Energy Agency Institutional Repository

Title	Negative Te spin polarization responsible for ferromagnetic order in the doped topological insulator $V_{0.04}(Sb_{1-x}Bi_x)_{1.96}Te_3$
Author(s)	Ye M., Xu T., Li G., Qiao S., Takeda Yukiharu, Saito Yuji, Zhu S.-Y., Nurmamat M., Sumida Kazuki, Ishida Yukiaki, Shin S., Kimura Akio
Citation	Physical Review B,99(14),p.144413_1-144413_7
Text Version	Published Journal Article
URL	https://jopss.jaea.go.jp/search/servlet/search?5065230
DOI	https://doi.org/10.1103/PhysRevB.99.144413
Right	ⓒ2019 American Physical Society

Japan Atomic Energy Agency

Negative Te spin polarization responsible for ferromagnetic order in the doped topological insulator $V_{0.04}(Sb_{1-x}Bi_x)_{1.96}Te_3$

M. Ye,[1,2,*] T. Xu,[1,2,3] G. Li,[4,†] S. Qiao,[1,2,4] Y. Takeda,[5] Y. Saitoh,[5] S.-Y. Zhu,[6] M. Nurmamat,[6] K. Sumida,[6] Y. Ishida,[7] S. Shin,[7] and A. Kimura[6,‡]

[1]*State Key Laboratory of Functional Materials for Informatics, Shanghai Institute of Microsystem and Information Technology, Chinese Academy of Sciences, Shanghai 200050, China*

[2]*CAS Center for Excellence in Superconducting Electronics (CENSE), Shanghai 200050, People's Republic of China*

[3]*University of Chinese Academy of Sciences, Beijing 100049, People's Republic of China*

[4]*School of physical science and technology, ShanghaiTech University, Shanghai 201210, People's Republic of China*

[5]*Materials Sciences Research Center, Japan Atomic Energy Agency. Hyogo 679-5148, Japan*

[6]*Graduate School of Science, Hiroshima University, 1-3-1 Kagamiyama, Higashi-Hiroshima, 739-8526, Japan*

[7]*ISSP, University of Tokyo, 5-1-5, Kashiwa-no-ha, Chiba 277-8581, Japan*

(Received 6 August 2018; revised manuscript received 8 March 2019; published 16 April 2019)

Ferromagnetic topological insulators have emerged as a promising platform for quantum anomalous Hall (QAH) effect with a dissipationless edge transport. However, the observation of QAH effect has so far been restricted to extremely low temperatures. We investigate the microscopic origin of ferromagnetism coupled with topological insulators in vanadium-doped $(Sb, Bi)_2Te_3$ employing the x-ray magnetic circular dichroism, angle-resolved two-photon photoemission spectroscopy, combined with first-principles calculations. We found a negative spin polarization, and thus an antiparallel magnetic moment at the Te site with respect to that of the vanadium dopants, which plays the key role in the ferromagnetic order. We ascribe it to the hybridization between Te p and V d majority spin states at the Fermi energy (E_F), being supported by a Zener-type p-d exchange interaction scenario. The substitution of Bi at the Sb site suppresses the bulk ferromagnetism by introducing extra electron carriers in the majority spin channel of Te p states that compensates the antiparallel magnetic moment on the Te site. Our findings reveal important clues to designing magnetic topological insulators with higher Curie temperature that work under ambient conditions.

DOI: 10.1103/PhysRevB.99.144413

I. INTRODUCTION

The discovery of the quantum Hall effect introduced topological concepts into condensed matter physics [1], in which integer values of the quantized Hall conductivity were later determined to express certain topological invariants (Chern numbers) [2]. The quantum Hall effect is characterized by a dissipationless edge current that results from Landau level splitting but requires strong external magnetic fields and samples of extremely high-electron mobility. The quantum anomalous Hall (QAH) effect can be regarded as a quantum Hall effect that takes place in the absence of an external magnetic field. It is predicted to occur in topological insulators (TIs) coupled with ferromagnetism, where the surface Dirac band exhibits an energy gap arising from broken time-reversal symmetry and provides a fertile ground for realizing exotic quantum phenomena, including the QAH effect that is accompanied by dissipationless transport [3,4]. Numerous attempts have been made to incorporate magnetism into the TI family via surface and bulk doping [5–9], and the magnetic proximity effect [10,11]. The realization of ferromagnetism combined with the topologically nontrivial states was reported by several groups even with perpendicular magnetic anisotropy, which is prerequisite in breaking the time-reversal symmetry. However, the observation of the QAH effect has so far been restricted to the $(Sb, Bi)_2Te_3$ system doped with chromium (Cr) or vanadium (V) atoms, where the Cr and V atoms are selectively substituted into the Sb site [12,13]. As one of the most serious problems, the precise quantization of the Hall resistance at zero field remains confined to low temperatures (10–100 mK) [14–17]. Nevertheless, a great effort thus has actually been made to raise its temperature [18]. An ideal QAH effect has been achieved in V-doped $(Sb, Bi)_2Te_3$, showing a larger coercivity with an almost vanishing residual longitudinal resistance than those of Cr-doped samples. Thus identifying the magnetic interaction provides an important clue to understanding the ferromagnetism formed in TIs, which could significantly benefit the material engineering of system exhibiting a QAH effect at higher temperature.

Due to the diluted doping concentration, the distance between the magnetic moments is too large to yield the direct d-d exchange interaction. The ferromagnetic coupling mediated by the host carriers has recently been evidenced for Cr-doped TIs by clarifying the tiny magnetic moment of Sb $5p$ electrons through x-ray magnetic circular dichroism (XMCD) technique [19–21]. Despite several subsequent works performed for V-doped $(Sb, Bi)_2Te_3$, no conclusive

*yemao@mail.sim.ac.cn
†ligang@shanghaitech.edu.cn
‡akiok@hiroshima-u.ac.jp

 ©2019 American Physical Society

physical picture has been obtained mainly due to a lack of the experimental investigation of the Te $5p$ magnetic states [20–22]. In addition, a partial substitution of Sb for Bi in the Sb_2Te_3 host could efficiently tune the bulk carriers [23]. Besides, the spontaneous ferromagnetism combined with the lack of bulk charge carriers brings about the QAH effect in TIs [3,4]. Therefore the interplay between the ferromagnetism and the bulk/surface carrier density should be scrutinized for V-doped samples in order to get comprehensive insight into their microscopic origin.

In this paper, we propose the exchange interaction of the vanadium-doped TI, $V_{0.04}(Sb_{1-x}Bi_x)_{1.96}Te_3$ ($x = 0$, 0.2, 0.3), which is a promising platform as a stable QAH system compared to the Cr-doped TIs. Using XMCD as an element-specific technique, we probed the magnetic moments induced at the Te and Sb sites of the host lattice in the presence of V dopants. The observed XMCD revealed that the magnetic moments at the Te site are aligned antiparallel to those at the Sb site and V dopants, signifying a negative spin polarization at the Te site, implying that the *p-d* exchange interaction is responsible for its ferromagnetism. We further demonstrate from two-photon photoemission (2PPE) measurements that the substitution of Sb for Bi results in a reduced hole carrier density, shifting the Fermi energy (E_F) closer to the Dirac point. Furthermore, our *ab initio* calculations reveal that the majority-spin channel of the Te $5p$ partial density of states (DOS) is pushed above the E_F via the hybridization with the V d states, which leads to the antiparallel coupled magnetic moment at the Te site.

II. EXPERIMENTAL METHODS

The XMCD experiments were performed at the twin-helical-undulator beamline BL23SU of SPring-8, where the fast switching of the x-ray helicity at 1 Hz enables data acquisition with an excellent signal-to-noise ratio [24]. The x-ray absorption (XAS) and XMCD spectra were acquired in a total-electron-yield mode in ultrahigh vacuum (better than 5×10^{-9} Pa). The 2PPE measurements were performed at a laser-based angle-resolved photoelectron spectroscopy station of the Institute for Solid State Physics, the University of Tokyo, employing the pump-probe technique with 1.48-eV pump and 5.92-eV probe laser pulses at a repetition rate of 250 kHz. The total energy resolution of 2PPE measurements was set to 15 meV; spectral broadening from the space charge effects was minimized to 10 meV [25]. The bulk single crystals of $V_{0.04}(Sb_{1-x}Bi_x)_{1.96}Te_3$ were grown following the modified Bridgman method and were carefully examined through XRD measurements that excluded a clustering of vanadium prior to the experiments. For all the measurements, the contamination-free sample surfaces were obtained by cleaving in ultrahigh vacuum.

III. RESULTS AND DISCUSSION

Figure 1(a) shows the normalized XAS spectra measured by circularly polarized x-rays at the V L_{23} ($2p \rightarrow 3d$) and Sb M_{45} ($3d \rightarrow 5p$) absorption edges of $V_{0.04}Sb_{1.96}Te_3$ ($T_C = 19$ K) with remnant magnetization perpendicular to the surface plane at 5 K. A clear difference is observed between the V L_{23} XAS spectra measured with opposite photon helicities, and indicates the appearance of dichroic signals of the V dopants. The resulting XMCD line shape obtained by taking the difference of these normalized XAS spectra is rather complicated due to a partial overlap of the L_2 and L_3 edges, which is similar to those reported recently [20,22], and is well described by the V^{3+} ion ($3d^2$) final state multiplets with a crystal field of $10Dq = 1$ eV [26]. In contrast, the XAS spectra only show a subtle difference at the Sb M_{45} edges measured with opposite photon helicities. However, the XMCD spectrum [Fig. 1(b)] at the Sb M_{45} edges presents clear dichroic signals, the intensity of which is about ~1% of the XAS (estimated by the edge jump at Sb M_{45}), with the opposite sign for the M_5 and M_4 edges, signifying the presence of magnetic moments at the Sb sites even with remnant magnetization. Most importantly, a clear XMCD intensities at the Te M_{45} absorption edges are observed [Figs. 1(c) and 1(d)], certainly demonstrating a presence of the induced magnetic moment at the Te site.

It is important to note that the XMCD spectra of Te and Sb edges exhibit opposite signs, even though they all correspond to the $3d \rightarrow 5p$ transitions. This indicates that the magnetic moments at the Te and Sb sites are coupled antiparallel. Considering that the XMCD at the L_{23} edges for the V dopant are related to the $2p \rightarrow 3d$ transition, the opposite signs between the V L_{23} and Sb M_{45} XMCD spectra demonstrates that the magnetic moment at the Sb site is aligned parallel to that of V dopant substituted in the same atomic layer, whereas the magnetic moment at the Te layer is aligned antiparallel [Fig. 1(e)] [27–29].

To add further details to this complicated magnetic coupling between the V dopants and the host lattice, we measured the XMCD intensity at V L_3, Sb M_5, and Te M_5 edges as a function of external magnetic field (M-H curve) applied perpendicular to the surface plane. As shown in Fig. 1(f), the XMCD intensities exhibit clear hysteresis loops for all three elements with a nonzero intensity at zero magnetic field, indicating spontaneous magnetization in both the dopant and the host lattice. For all three elements, the widths of the hysteresis loops are equivalent implying that the magnetic moments are strongly coupled. The coexistence of parallel and antiparallel coupling of the moments in V-doped $(Sb, Bi)_2Te_3$ is strongly supported by the Zener-type *p-d* exchange interaction scenario, in which the hybridization between the Te p states and the V d valence states plays an essential role [30–32]. This interaction is also accompanied by an indirect exchange interaction within each quintuple layers parallel to the (0001) [Fig. 1(e)] surface mediated by the free carriers and leads to a parallel spin coupling between the Sb $5p$ states and the V $3d$ states [33].

By increasing the Bi concentration in $V_{0.04}(Sb_{1-x}Bi_x)_{1.96}Te_3$ from 0 to 0.2 and 0.3, T_C experiences an abrupt drop from 19 to 14 K and 8.5 K, respectively. From the XMCD spectra measured for the samples with different Bi concentrations at the V, Sb, and Te absorption edges normalized by the XAS intensities [Figs. 2(a)–2(c)], their rapid decreases are in good agreement with the decreasing T_C arising from the Bi doping effect. For $x = 0.2$, all the XMCD spectra are well reproduced at the absorption edge of each element, but the XMCD signal weakens considerably for

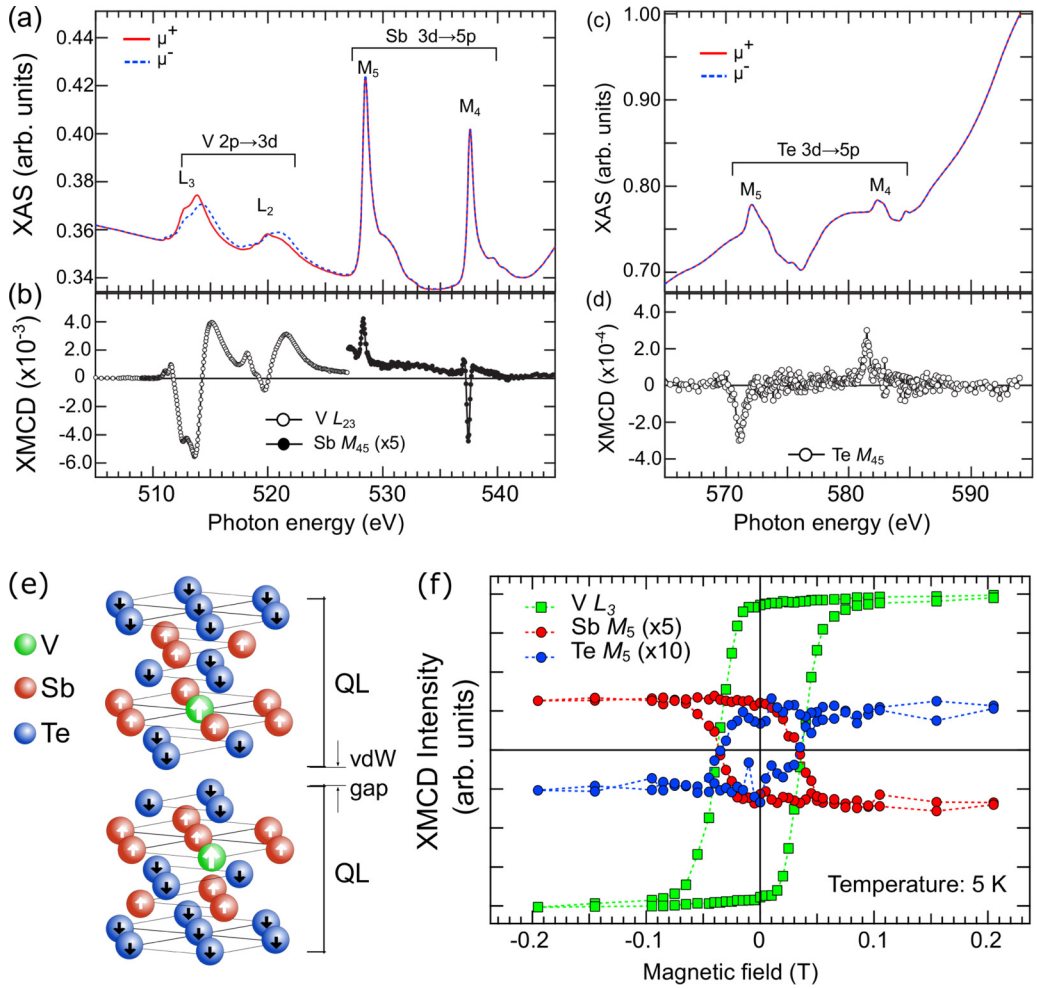

FIG. 1. (a) XAS and (b) XMCD spectra of $V_{0.04}Sb_{1.96}Te_3$ measured at V L_{23} and Sb M_{45} edges at 5 K with out-of-plane remnant magnetization. (c) and (d), same as (a) and (b) for Te M_{45} edges.(e) Crystal structure of $V_{0.04}Sb_{1.96}Te_3$ crystal with magnetic moments on each atom. (f) XMCD amplitudes at the V L_3, Sb M_5, and Te M_5 edges plotted as a function of applied magnetic field.

$x = 0.3$ sample. The M-H curves for different x at V L_3, Sb M_5, and Te M_5 edges [Figs. 2(d)–2(f)] exhibit clear magnetic hysteresis loops. For $x = 0.2$, it shows only a half of the width of the hysteresis loops compared with $x = 0$ sample at the corresponding edges. These results confirm that the substitutional Bi atoms significantly suppress the long-range magnetic order.

To better understand the exchange interaction being responsible for the ferromagnetic ordering in the V-doped topological insulator, the underlying mechanism for the abrupt suppression of ferromagnetism on the Bi substitution at the Sb site needs to be revealed. Note that the topological surface states (TSSs) are mostly located above the E_F due to the host p-type carriers induced by the Sb-Te antisite defects [23,34]. Therefore the conventional ARPES cannot access to the TSSs in the unoccupied states. Besides, the existence of TSSs is not guaranteed in the presence of magnetic impurities. The electronic states near the E_F were then investigated using the 2PPE for $V_{0.04}(Sb_{1-x}Bi_x)_{1.96}Te_3$. For the sample without Bi substitution, the E_F intersects the bulk valence band, and the whole TSS is unoccupied, in which no Dirac-cone-like dispersions are seen[left panel of Fig. 3(a)]. The spectrum acquired from $V_{0.04}Sb_{1.96}Te_3$ after the pump pulse arrives [right panel of Fig. 3(a)] shows that the TSSs in the unoccupied state region can be probed with its Dirac point located at energy (E_D) of 173 meV (white dashed line) above the E_F (black dashed line). After Bi substitution on the Sb site by 20%, the Dirac point shifts downward to $E_D = 65$ meV as a consequence of the n-type carriers induced by Te vacancy naturally formed with Bi substitution [23,34]. A further increase in the concentration of Bi to 30% lowers the Dirac point by 35 meV with E_F located in the bulk energy gap [Figs. 3(b) and 3(c)]. However, due to the limited energy resolution (∼15 meV) in the 2PPE experiment, the opening of an energy gap at the Dirac point could not be clearly judged. Nevertheless, although increasing the Bi concentration effectively reduces the bulk carrier concentration while maintaining the presence of TSSs as demonstrated in Figs. 3(b) and 3(c), it is accompanied by a sudden suppression of ferromagnetism as in the case of Cr-doped $(Sb, Bi)_2Te_3$ [19], resulting in an abrupt decrease of the Curie temperature [Fig. 3(d)]. This behavior is not accommodated by the proposed Van Vleck-type ferromagnetism, which is independent of the bulk carrier density [4]. Such a dependence of ferromagnetism on carrier density also differs

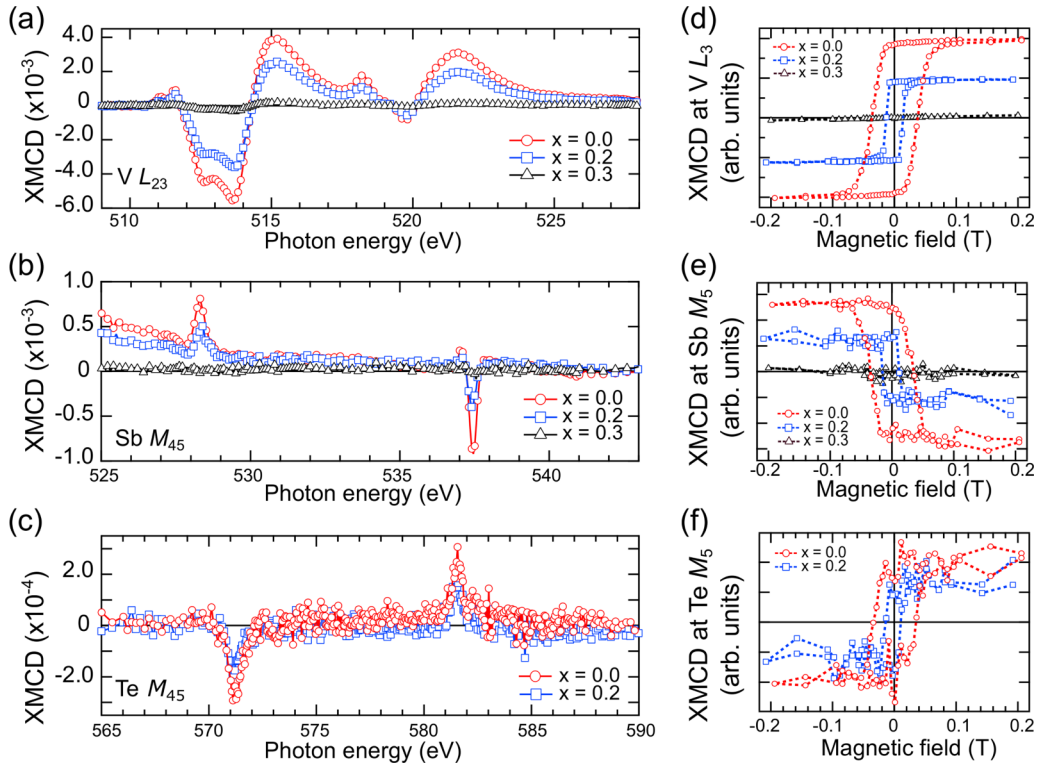

FIG. 2. XMCD spectra of $V_{0.04}(Sb_{1-x}Bi_x)_{1.96}Te_3$ measured at (a) V L_{23}, (b) Sb M_{45} and (c) Te M_{45} edges, respectively, for $x = 0$, 0.2, and 0.3 samples at 5 K. XMCD intensities at (d) V L_3, (e) Sb M_5, and (f) Te M_5 edges as functions of applied magnetic field for corresponding samples measured at 5 K.

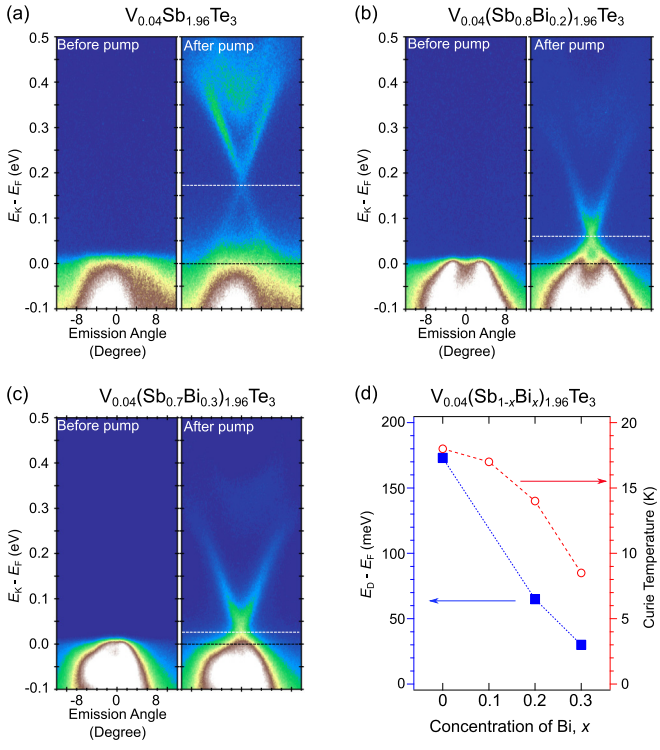

FIG. 3. Topological surface state dispersions in the unoccupied states region of $V_{0.04}(Sb_{1-x}Bi_x)_{1.96}Te_3$ probed by 2PPE measurements for (a) $x = 0$, (b) 0.2, and (c) 0.3 along $\bar{\Gamma}$-$\bar{M}$ direction at a temperature of 3.3 K. (d) Binding energy of Dirac point and the Curie temperatures as the function of Bi concentration.

from a previous report on V-doped Sb_2Te_3, where a type of Van Vleck picture dominated by the contribution from the core states of V is responsible for the ferromagnetism [35].

IV. THEORETICAL CALCULATION

To gain a deeper insight into the competition between carrier tuning and ferromagnetism, investigating the impurity states in analogy to the diluted magnetic semiconductors is important, especially the energy of the V d states relative to the E_F and the bulk energy gap of the host materials [31,32]. According to Ref. [36], the surface-electron mediated Ruderman-Kittel-Kasuya-Yosida (RKKY) mechanism can result in an antiparallel magnetic coupling unless the Dirac point is located close to the Fermi level. However, no antiferromagnetic coupling has been detected among the V dopant. In addition, since the bulk carrier density in the studied system is rather small, the RKKY interaction can hardly be accounted for the magnetism in V-doped $(Sb, Bi)_2Te_3$. We then performed first-principles calculations based on the supercell method for the V-doped Sb_2Te_3 sample, in which a $4 \times 4 \times 3$ supercell including 144 Te atoms, 94 Sb atoms, and 2 V atoms was configured to simulate the $V_{0.04}Sb_{1.96}Te_3$ sample. To account for all symmetry-inequivalent positions of the V dopants inside the supercell, we generated 30 different structures, the density of states (DOS) of which were calculated using the Vienna *ab initio* simulation package [37], with the generalized gradient approximation [38] as exchange-correlation functional and a $2 \times 2 \times 2$ k mesh. To probe the magnetic polarization induced by the V dopants in

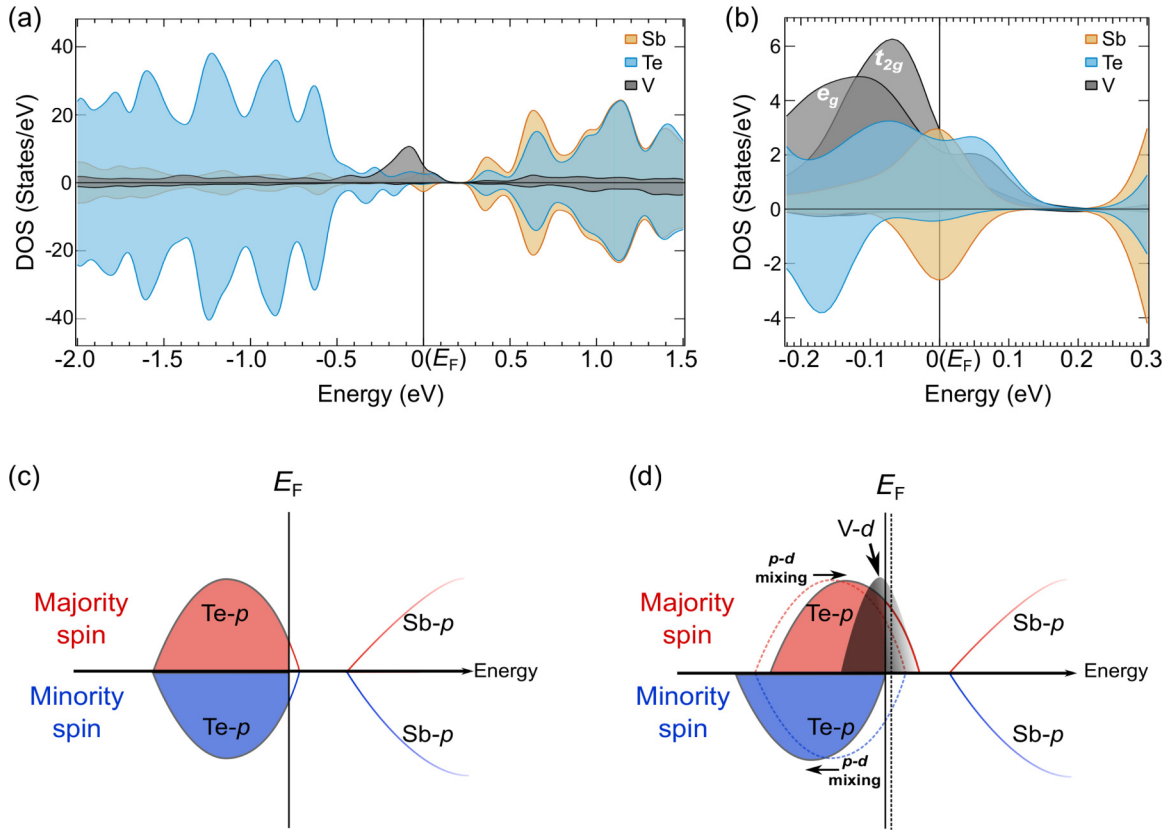

FIG. 4. (a) Calculated spin-polarized DOS of $V_{0.04}Sb_{1.96}Te_3$. (b) Calculated DOS in the vicinity of E_F. Schematic band diagram of Sb_2Te_3 (c) before and (d) after V doping.

our calculations, spin symmetry breaking was allowed for all atoms inside the super-cell. Highly consistent with the experiment, we found that the doped V induces a ferromagnetic correlation with Sb and an antiferromagnetic correlation with Te. The calculated DOS was averaged over all the structures [Fig. 4(a)], showing E_F intersecting the bulk valence band. Importantly, a sharp peak originating from the majority spin states of V is found to be located at an energy of ∼0.1 eV below E_F, which is consistent with previously reported resonant soft x-ray photoelectron spectroscopy results [39,40]. This band diagram is quite similar to that for the well-known diluted magnetic semiconductor, $Ga_{1-x}Mn_xAs$, in which the impurity band formed by Mn 3d electrons is located at the valence band top of the host GaAs below the E_F [41]. An amplified view of the DOS near E_F [Fig. 4(b)] reveals a strong hybridization between the Te p and V d states in the majority spin channel around E_F. The t_{2g} and e_g states of the V d electrons are slightly split, and both extended to unoccupied states. Consequently, a strong hybridization (p-d mixing) between the Te p and V d states pushes the majority spin component of Te p states above the E_F. This hybridization reduces the occupancy of the Te p majority spin states, which results in an antiparallel magnetic moment at the Te site, as probed by our XMCD experiments. On the other hand, the Sb p states are dominant in the conduction band region, and a weak V d - Sb p mixing in the same plane slightly enhances the majority spin DOS below E_F [Fig. 4(a)], resulting in a small but parallel moment with respect to the V dopants.

Hence, the mechanism behind the magnetic interaction in V-doped Sb_2Te_3 follows a prescribed scheme [Figs. 4(c) and 4(d)]. Firstly, the strong hybridization between the V d states and Te p states pushes the majority spin component of the Te p band to a higher energy, resulting in antiparallel moments at the Te site. This exchange interaction mechanism is dominated by the V-V interactions in the V-doped $(Sb, Bi)_2Te_3$ via an anion (Te) layer between the magnetic dopants (V) in different cation (Sb) layers. Meanwhile, the spin splitting of the Te p states can also stabilize the V-doped Sb_2Te_3 system by shifting the E_F to a lower energy as indicated in Fig. 4(d). Secondly, a co-existing indirect exchange mechanism via free carriers in the same cation (Sb) layers gives rise to the parallel magnetic moment on Sb sites with respect to the V dopants. However, this interaction is relatively weaker, and thus plays less important role in the formation of long range magnetic order in V-doped $(Sb, Bi)_2Te_3$.

Finally, we discuss the effect of Bi substitutions at the Sb site. Partial substitution of Sb by Bi induces extra bulk electron carriers that can push the E_F into the bulk energy gap, which is crucial to realize the QAH effect. However, this process results in an abrupt decrease in the bulk magnetism [Fig. 3(d)]. This phenomenon can be understood from the schematic diagram [Fig. 4(d)], where the tuning of E_F towards the bulk energy gap increases the occupancy of the Te p majority spin states while almost maintaining the occupancy of the minority spin states through spin splitting of the Te p states. Therefore the magnetic moments at the Te sites are reduced accompanied by a tuning of E_F and are eventually

eliminated when E_F shifts into the bulk energy gap. As a consequence, long-range magnetic ordering in the bulk crystal is strongly suppressed due to the reduced magnetic moments in the host lattice that mediated the local magnetic moment among V impurities. Nevertheless, the strong hybridization between Te/Sb p and V d may still play a role in the formation of ferromagnetism, but this role needs to be further investigated.

V. CONCLUSION

To conclude, with XMCD measurements taken from V-doped $(Sb, Bi)_2Te_3$, we revealed that antiparallel magnetic moments on the Te sites with respect to the Sb and V sites are crucial for the formation of long-range magnetic ordering. Our theoretical investigation unambiguously reveals that such ferromagnetism in dilute magnetic TIs are ascribable to a strong hybridization between the Te p and V d majority spin states. This hybridization results in a shift in the Te p majority spin states to unoccupied states, which consequently leads to an antiparallel magnetic moment and a negative spin polarization at the Te site. The substitution of Bi at the Sb site undermines the long-range magnetic ordering by reducing the magnetic moment at the Te site. Our findings provide important clues to understand the origin of ferromagnetism in magnetically doped TIs and pave the way for the realization by material engineering of the QAH effect at much higher temperatures through the tuning of the magnetic exchange interactions.

ACKNOWLEDGMENTS

This work was supported by National Key R&D Program of China (2017YFA0305400), and the Natural Science Foundation of China (Grants No. 11227902 and No. U1632266). The XMCD/XAS experiments were performed at SPring-8 under the Shared Use Program of JAEA Facilities with the approval of Nanotechnology Platform project supported by the Ministry of Education,Culture, Sports, Science and Technology (Proposals No. 2015A3880, No. 2015B3880, and No. 2016A3830). 2PPE experiment was conducted under the permission of the joint research in ISSP, the University of Tokyo. A. K. acknowledges the financial support by JSPS Kakenhi (Grants No. 17H06138 and No. 18H03683). G. L. acknowledges the starting grant of ShanghaiTech University and Program for Professor of Special Appointment (Shanghai Eastern Scholar). Calculations were carried out at the HPC Platform of Shanghaitech University Library and Information Services, and School of Physical Science and Technology.

[1] K. V. Klitzing, G. Dorda, and M. Pepper, Phys. Rev. Lett. **45**, 494 (1980).
[2] D. J. Thouless, M. Kohmoto, M. P. Nightingale, and M. den Nijs, Phys. Rev. Lett. **49**, 405 (1982).
[3] X.-L. Qi, Y.-S. Wu, and S.-C. Zhang, Phys. Rev. B **74**, 085308 (2006).
[4] R. Yu, W. Zhang, H.-J. Zhang, S.-C. Zhang, X. Dai, and Z. Fang, Science **329**, 61 (2010).
[5] J. G. Checkelsky, J. Ye, Y. Onose, Y. Iwasa, and Y. Tokura, Nat. Phys. **8**, 729 (2012).
[6] F. Yang, Y. R. Song, H. Li, K. F. Zhang, X. Yao, C. Liu, D. Qian, C. L. Gao, and J.-F. Jia, Phys. Rev. Lett. **111**, 176802 (2013).
[7] L. A. Wray, S.-Y. Xu, Y. Xia, D. Hsieh, A. V. Fedorov, Y. S. Hor, R. J. Cava, A. Bansil, H. Lin, and M. Z. Hasan, Nat. Phys. **7**, 32 (2011).
[8] M. R. Scholz, J. Sánchez-Barriga, D. Marchenko, A. Varykhalov, A. Volykhov, L. V. Yashina, and O. Rader, Phys. Rev. Lett. **108**, 256810 (2012).
[9] J. Honolka, A. A. Khajetoorians, V. Sessi, T. O. Wehling, S. Stepanow, J.-L. Mi, B. B. Iversen, T. Schlenk, J. Wiebe, N. B. Brookes, A. I. Lichtenstein, Ph. Hofmann, K. Kern, and R. Wiesendanger, Phys. Rev. Lett. **108**, 256811 (2012).
[10] I. Vobornik, U. Manju, J. Fujii, F. Borgatti, P. Torelli, D. Krizmancic, Y. S. Hor, R. J. Cava, and G. Panaccione, Nano Lett. **11**, 4079 (2011).
[11] S. V. Eremeev, V. N. Men'shov, V. V. Tugushev, P. M. Echenique, and E. V. Chulkov, Phys. Rev. B **88**, 144430 (2013).
[12] J. S. Dyck, P. Hájek, P. Lošt'ák, and C. Uher, Phys. Rev. B **65**, 115212 (2002).
[13] C.-Z. Chang, J. Zhang, M. Liu, Z. Zhang, X. Feng, K. Li, L.-L. Wang, X. Chen, X. Dai, Z. Fang, X.-L. Qi, S.-C. Zhang, Y. Wang, K. He, X.-C. Ma, Q.-K. Xue, Adv. Mater. **25**, 1065 (2013).
[14] C.-Z. Chang, J. Zhang, X. Feng, J. Shen, Z. Zhang, M. Guo, K. Li, Y. Ou, P. Wei, L.-L. Wang, Z.-Q. Ji, Y. Feng, S. Ji, X. Chen, J. Jia, X. Dai, Z. Fang, S.-C. Zhang, K. He, Y. Wang, L. Lu, X.-C. Ma, Q.-K. Xue, Science **340**, 167 (2013).
[15] X. Kou, S.-T. Guo, Y. Fan, L. Pan, M. Lang, Y. Jiang, Q. Shao, T. Nie, K. Murata, J. Tang, Y. Wang, L. He, T.-K. Lee, W.-L. Lee, and K. L. Wang, Phys. Rev. Lett. **113**, 137201 (2014).
[16] A. J. Bestwick, E. J. Fox, X. Kou, L. Pan, K. L. Wang, and D. Goldhaber-Gordon, Phys. Rev. Lett. **114**, 187201 (2015).
[17] C.-Z. Chang, W. Zhao, D. Y. Kim, H. Zhang, B. A. Assaf, D. Heiman, S.-C. Zhang, C. Liu, Moses H. W. Chan, and J. S. Moodera, Nat. Mat. **14**, 473 (2015).
[18] W. Li, M. Claassen, C.-Z. Chang, B. Moritz, T. Jia, C. Zhang, S. Rebec, J. J. Lee, M. Hashimoto, D.-H. Lu, R. G. Moore, J. S. Moodera, T. P. Devereaux, and Z.-X. Shen, Sci. Rep. **6**, 32732 (2016).
[19] M. Ye, W. Li, S. Zhu, Y. Takeda, Y. Saitoh, J. Wang, H. Pan, M. Nurmamat, K. Sumida, F. Ji, Z. Liu, H. Yang, Z. Liu, D. Shen, A. Kimura, S. Qiao, and X. Xie, Nat. Commun. **6**, 8913 (2015).
[20] M. F. Islam, C. M. Canali, A. Pertsova, A. Balatsky, S. K. Mahatha, C. Carbone, A. Barla, K. A. Kokh, O. E. Tereshchenko, E. Jiménez, N. B. Brookes, P. Gargiani, M. Valvidares, S. Schatz, T. R. F. Peixoto, H. Bentmann, F. Reinert, J. Jung, T. Bathon, K. Fauth, M. Bode, and P. Sessi, Phys. Rev. B **97**, 155429 (2018).
[21] L. B. Duffy, A. I. Figueroa, G. van der Laan, and T. Hesjedal, Phys. Rev. Mater. **1**, 064409 (2017).
[22] Paolo Sessi, R. R. Biswas, T. Bathon, O. Storz, S. Wilfert, A. Barla, K. A. Kokh, O. E. Tereshchenko, K. Fauth,

M. Bode, and A. V. Balatsky, Nat. Commun. **7**, 12027 (2016).
[23] J. Zhang, C.-Z. Chang, Z. Zhang, J. Wen, X. Feng, K. Li, M. Liu, K. He, L. Wang, X. Chen, Q.-K. Xue, X. Ma, and Y. Wang, Nat. Commun. **2**, 574 (2011).
[24] Y. Saitoh, Y. Fukuda, Y. Takeda, H. Yamagami, S. Takahashi, Y. Asano, T. Hara, K. Shirasawa, M. Takeuchi, T. Tanaka, and H. Kitamura, J. Synchrotron Rad. **19**, 388 (2012).
[25] Y. Ishida, T. Togashi, K. Yamamoto, M. Tanaka, T. Kiss, T. Otsu, Y. Kobayashi, and S. Shin, Rev. Sci. Instrum. **85**, 123904 (2014).
[26] G. van der Laan and B. T. Thole, Phys. Rev. B **43**, 13401 (1991).
[27] W. L. O'Brien and B. P. Tonner, Phys. Rev. B **50**, 12672 (1994).
[28] A. Kimura, S. Suga, T. Shishidou, S. Imada, T. Muro, S. Y. Park, T. Miyahara, T. Kaneko, and T. Kanomata, Phys. Rev. B **56**, 6021 (1997).
[29] S. S. Dhesi, H. A. Dürr, G. van der Laan, E. Dudzik, and N. B. Brookes, Phys. Rev. B **60**, 12852 (1999).
[30] C. Zener, Phys. Rev. **81**, 440 (1951).
[31] T. Dietl, H. Ohno, F. Matsukura, J. Cibert, and D. Ferrand, Science **287**, 1019 (2000).
[32] K. Sato, L. Bergqvist, J. Kudrnovsky, P. H. Dederichs, O. Eriksson, I. Turek, B. Sanyal, G. Bouzerar, H. Katayama-Yoshida, V. A. Dinh, T. Fukushima, H. Kizaki, and R. Zeller, Rev. Mod. Phys. **82**, 1633 (2010).
[33] M. G. Vergniory, M. M. Otrokov, D. Thonig, M. Hoffmann, I. V. Maznichenko, M. Geilhufe, X. Zubizarreta, S. Ostanin, A. Marmodoro, J. Henk, W. Hergert, I. Mertig, E. V. Chulkov, and A. Ernst, Phys. Rev. B **89**, 165202 (2014).
[34] G. Wang, X.-G. Zhu, Y.-Y. Sun, Y.-Y. Li, T. Zhang, J. Wen, X. Chen, K. He, L.-L. Wang, X.-C. Ma, J.-F. Jia, S. B. Zhang, Q.-K. Xue, Adv. Mater. **23**, 2929 (2011).
[35] M. Li, C.-Z. Chang, L. Wu, J. Tao, W. Zhao, Moses H. W. Chan, J. S. Moodera, J. Li, and Y. Zhu, Phys. Rev. Lett. **114**, 146802 (2015).
[36] Q. Liu, C.-X. Liu, C. Xu, X.-L. Qi, and S.-C. Zhang, Phys. Rev. Lett. **102**, 156603 (2009).
[37] G. Kresse, J. Furthmüller, Phys. Rev. B **54**, 11169 (1996).
[38] J. P. Perdew, K. Burke, and M. Ernzerhof, Phys. Rev. Lett. **77**, 3865 (1996).
[39] T. R. F. Peixoto, H. Bentmann, S. Schreyeck, M. Winnerlein, C. Seibel, H. Maaß, M. Al-Baidhani, K. Treiber, S. Schatz, S. Grauer, C. Gould, K. Brunner, A. Ernst, L. W. Molenkamp, and F. Reinert, Phys. Rev. B **94**, 195140 (2016).
[40] J. A. Krieger, C.-Z. Chang, M.-A. Husanu, D. Sostina, A. Ernst, M. M. Otrokov, T. Prokscha, T. Schmitt, A. Suter, M. G. Vergniory, E. V. Chulkov, J. S. Moodera, V. N. Strocov, and Z. Salman, Phys. Rev. B **96**, 184402 (2017).
[41] M. Kobayashi, I. Muneta, Y. Takeda, Y. Harada, A. Fujimori, J. Krempaský, T. Schmitt, S. Ohya, M. Tanaka, M. Oshima, and V. N. Strocov, Phys. Rev. B **89**, 205204 (2014).